This article has been accepted for publication in IEEE Antennas and Wireless Propagation Letters. This is the author's version which has not been fully edited and content may change prior to final publication. Citation information: DOI 10.1109/LAWP.2024.3489426

2D FEM-Based Simulation and Optimization of Concentric Ring GRIN Lens Antennas

J.M. Poyanco, *Student Member, IEEE*, R. Gómez Alcalá, *Member, IEEE*, F. Pizarro, *Senior Member, IEEE*, E. Rajo-Iglesias, *Senior Member, IEEE*, J. M. Gil, J. Rubio

***Abstract*—In this work, a hybridized 2D Finite Element Method (FEM) with modal analysis is used to study a flat 3D Gradient-Index (GRIN) dielectric lens with a diameter of $10\lambda_0$. The use of this memory-efficient and fast method allows parametric studies or even optimization of the lens, which is generally not feasible using commercial full-wave simulators. Thanks to this tool, in a first study, the effect of the number of rings constituting the lens on its performance is analyzed whilst in a second step, a genetic algorithm is used to optimize the width of each ring to obtain a higher gain at three frequencies within the frequency band. Finally, the focal distance, lens thickness, and maximum permittivity are optimized to maximize the realized gain, while imposing constraints on the Sidelobe Levels (SLL) and reflection coefficient levels.**

***Index Terms*—GRIN lens, FEM 2D, concentric rings lens, dielectric lens antennas, genetic algorithm.**

I. Introduction

Lens antennas are emerging as a powerful option for the next generations of wireless communications networks [1]. Among the various types available, notable examples include geodesic lens antennas [2]–[4], dielectric or metallic meta-lens antennas embedded in a parallel plate structure [5]–[7] or three-dimensional dielectric lens [8]–[10]. Historically, dielectric lenses have been considered bulky, heavy, and exhibited high losses [11]. These issues can be addressed with tools such as transformation optics [12] or by designing planar lenses [13]. Additionally, dielectric lenses with reduced weight can be produced using 3D-printing with dielectric filaments mixed with air [14]–[16]. Moreover, it has been demonstrated that currently available filaments in the industry exhibit low losses, even when used at high-frequency bands, enabling their use in fabricating various dielectric planar lenses [15].

Regarding GRIN lenses, one commonly used type comprises dielectric rings that compensate for the optical paths to achieve a plane wavefront at the lens output. These lenses are designed using principles of optical physics [17], [18], and there have been various studies investigating such lenses. These include applications for the K_u-band [17], [19], K and K_a-bands [18], [20]–[23], and even the W-band [24]. Of particular interest is the study presented in [20], where the feed antenna and its radiation characteristics are considered in the lens design, allowing for the calculation of the optimal lens position relative to the feed to achieve the highest possible aperture efficiency. In previous work from the authors, one of these lenses has been implemented using 3D-printing as a prototyping method [25]. For this lens, the center frequency was 34 GHz and its operational bandwidth covered the entire K_a-band.

In the design of lens antennas, it is common practice to discretize the lens using concentric rings of equal width based on well-established equations. However, exploring variations in ring widths, as well as other parameters such as lens thickness and focal distance, can potentially enhance lens performance. Optimizing these variables is challenging due to the heavy computational demands associated with simulating hundreds or thousands of electrically large devices.

This work focuses on the application of a hybridized 2D full-wave FEM method, combined with modal analysis, to analyze and design lens antennas that exhibit rotational symmetry and field excitation with sinusoidal dependence [26]. The method provides a generalized scattering matrix for circular waveguide propagation modes in the feeding waveguide and spherical modes as a radiation boundary condition. The advantage of this approach lies in its efficient handling of electrically large lenses by leveraging the symmetry of the lens and feed antenna system, which significantly reduces computational resource requirements allowing unprecedented studies. The study begins by presenting the original lens design and the results obtained using the proposed 2D-FEM method. The emphasis is placed on how this approach allows for efficient exploration of various lens parameters, including the impact of concentric ring widths, lens thickness, and focal distance on performance. The study also explores non-intuitive results such as the effect of varying ring widths on gain at specific frequencies and the impact of ring discretization on performance. Finally, the optimization of lens parameters using a genetic algorithm is demonstrated, illustrating how considering the mutual interactions between the feed and lens enables the reduction of focal length and lens thickness compared to the theoretical optimum, resulting in a more compact and efficient lens design.

II. Method of analysis

Let's consider as example the lens presented in [25]. As shown in Fig. 1 (namely "Case 0"), the lens exhibits

This work has been partially funded by the Spanish Ministry of Science and Innovation (MCIN/AEI/ FEDER, EU) through the projects PID2021-122856NB-C21, PID2021-122856NB-C22, and PID2019-107688RB-C21, and ANID FONDEQUIP EQM220109.

J.M. Poyanco and E. Rajo-Iglesias are with the University Carlos III of Madrid, Department of Signal Theory and Communication, 28912, Madrid, Spain (e-mails: jpoyanco@pa.uc3m.es; eva.rajo@uc3m.es

R. Gómez Alcalá and J. Rubio are with University of Extremadura, Department of Computers and Communications Technology, 10003, Cáceres, Spain (e-mails: rgomezal@unex.es; jesusrubio@unex.es)).

J. M Gil is with the Technical University of Madrid, Department of Signals, Systems and Radiocommunications, 28040, Madrid, Spain (e-mail: jmg@etc.upm.es).

F. Pizarro is with the Pontificia Universidad Católica de Valparaíso, Escuela de Ingeniería Electrica, 2362804,Valparaiso, Chile (e-mail: francisco.pizarro.t@pucv.cl).

Authorized licensed use limited to: Biblioteca de la Universidad de Extremadura. Downloaded on December 20,2024 at 11:14:42 UTC from IEEE Xplore. Restrictions apply.
© 2024 IEEE. Personal use is permitted, but republication/redistribution requires IEEE permission. See https://www.ieee.org/publications/rights/index.html for more information.

This article has been accepted for publication in IEEE Antennas and Wireless Propagation Letters. This is the author's version which has not been fully edited and content may change prior to final publication. Citation information: DOI 10.1109/LAWP.2024.3489426

physical rotational symmetry, along with its feed, where the z axis serves as the axis of revolution, and φ represents the cylindrical azimuthal variable. Therefore, this lens-feed system could be analyzed using 3D FEM [27]. However, applying 3D FEM to such a study is computationally expensive due to the large electrical size of the lens under analysis ($10\lambda_0$) and consequently the domain that needs to be discretized using this method.

In the formulation of 3D FEM, considering the previously described rotational symmetry and excitation, the magnetic field to be approximated within the volume can be expressed as [27]:

$$\vec{H} = \sum_{m=0}^{\infty} \left[\vec{h}_\tau(r,z)\sin(m\varphi) + \hat{\varphi}\frac{1}{r}h_\varphi(r,z)\cos(m\varphi) \right] \quad (1)$$

while the tangential electric field at the ports will be given by the contribution of the different modes in which this field is expanded. In this case, each excitation mode j in each port p can be represented by:

$$\vec{e}_{tpj} = \vec{e}_{\tau pj}(r,z)\sin(m\varphi) + \hat{\varphi}e_{\varphi pj}(r,z)\cos(m\varphi) \quad (2)$$

By introducing these equations into the formulation of 3D FEM and integrating over φ, we can analytically remove the dependence on this variable, as long as a rotational symmetry exists. Consequently, it is reduced to a 2D FEM problem for each value of m [26]. In our design, the feed is excited by the fundamental mode of the circular waveguide, thus requiring the solution of a 2D FEM problem with $m = 1$ only.

To achieve accurate results, second-order curved triangular finite elements are employed to approximate the magnetic field in the (r, z) plane. The azimuthal component is approximated using second-order Lagrange polynomials, while the transverse component uses second-order tangential functions [28].

The solution of the 2D-FEM problem yields the generalized admittance matrix, from which it is straightforward to obtain the generalized scattering matrix of the lens-feed system. As explained in [29], this matrix directly provides the S_{11} parameter and the radiated field can be analytically obtained by summing all the spherical modes weighted by their transmission coefficients. These coefficients are the S_{21} parameters between the circular waveguide mode and every spherical mode. In addition, the radiated power is given by the sum of the square of the absolute value of the transmission parameters, as detailed in [29]. From the radiated field and the radiated power, the directivity is directly computed.

Fig. 2 illustrates an explanatory diagram of the 2D model applied to the lens and its feed.

III. Concentric Rings GRIN Lens Antenna

The design of the concentric ring GRIN lens is based on compensating for the different optical paths from the focal point F to the lens surface by assigning decreasing radial permittivities. The equation describing this compensation is shown in (3) [18]. The details of this compensation are shown below:

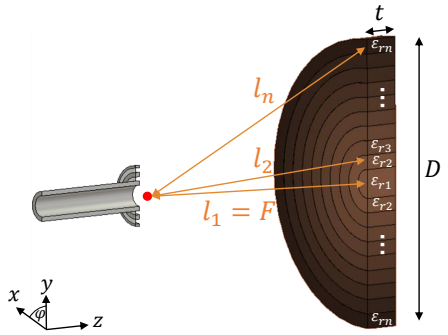

Fig. 1. Description of the original concentric ring GRIN lens.

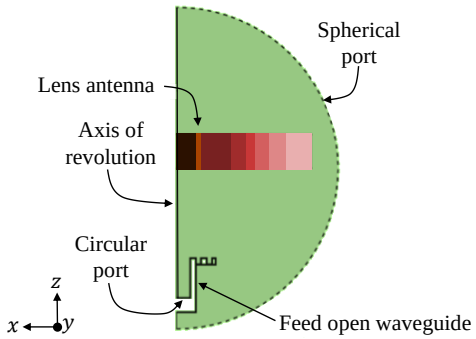

Fig. 2. 2D computational model of the lens antenna and its feed.

- Define the design parameters, such as the central operational frequency f_0, the total diameter D, lens thickness t, and focal distance F.
- Determine the total number of rings. Ideally, this lens has an infinite number of rings, exhibiting a continuous change in permittivity. However, since this is not achievable in practice, it is necessary to discretize the design by defining a total number of rings n, resulting in a ring thickness w_n equal to $D/(2n)$.
- Define the maximum (minimum) permittivity ε_1 (ε_n) located in the central (outermost) ring available for the prototyping of this lens.
- Calculate the permittivity of each ring ε_n:

$$\varepsilon_n = \left(\frac{l_1 - l_n + \sqrt{\varepsilon_1}t}{t} \right)^2 \quad (3)$$

  where l_n corresponds to the distance between the focal point F and the midpoint of each ring. If the minimum permittivity is chosen, in (3), replace l_1 with l_n and ε_1 with ε_n.

The lens antenna shown in [25] was designed, simulated, manufactured and measured and has the following parameters: an operating frequency f_0 of 34 GHz, a total diameter D of $10\lambda_0$ (88.24 mm), a thickness t of $D/8$ (11.03 mm), a focal distance F of $D/3$ (29.41 mm) and a total number of rings n equal to 10. Fig. 3 shows the realized gain simulated using CST Microwave Studio with two symmetry planes, along with a comparison to the results obtained with the method described in the previous section, both at 34 GHz. It is important to note that CST Studio was run on a dedicated server with 2x12 cores @3.5 GHz and 256 GB of RAM to obtain these results, while

Authorized licensed use limited to: Biblioteca de la Universidad de Extremadura. Downloaded on December 20,2024 at 11:14:42 UTC from IEEE Xplore. Restrictions apply.
© 2024 IEEE. Personal use is permitted, but republication/redistribution requires IEEE permission. See https://www.ieee.org/publications/rights/index.html for more information.

This article has been accepted for publication in IEEE Antennas and Wireless Propagation Letters. This is the author's version which has not been fully edited and content may change prior to final publication. Citation information: DOI 10.1109/LAWP.2024.3489426

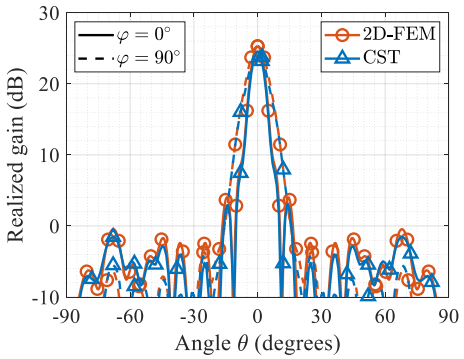

Fig. 3. E- and H- plane far-field radiation patterns of the lens at 34 GHz simulated using CST Studio and 2D FEM for $\varphi = 0^o$ and $\varphi = 90^o$.

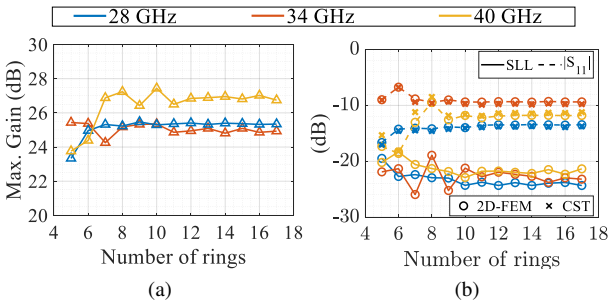

Fig. 4. Simulation results obtained at 28, 34, and 40 GHz for different numbers of rings. a) Maximum gain, b) reflection coefficient and SLL.

a laptop was used for the 2D FEM calculations. CST Studio took approximately 6 minutes to complete, while the 2D FEM calculation method provided results in less than 10 seconds.

Given that the results obtained with the 2D FEM align perfectly with those obtained with CST, we proceed to leverage this method to conduct a series of studies. These include analyzing the effects of the number of rings composing the lens, the width of each ring, the lens thickness, and focal distance on its performance.

IV. Analysis of the Number of Rings

The first proposed study is to analyze the effect of the number of rings used for discretizing the lens, while the other lens variables such as diameter D, thickness t, and focal distance F are kept constant. The permittivity values of each ring are recalculated for each case using (3).

Theoretically, it is necessary to achieve a continuous variation in phase compensation across the radius, ensuring that each point along the lens compensates its corresponding optical path with a different permittivity value. At first glance, it is easy to expect that by discretizing the lens into a larger number of rings, a better performance will be achieved.

To study the effect of this variable, several dielectric lenses with a number of rings in the range of 5 to 17 were analyzed. As shown in Fig. 4, for this example, increasing the number of rings beyond 8 does not lead to any noticeable improvement. With this number of rings, the maximum gain, reflection coefficient and SLL converge for the three analyzed frequencies within the K_a-band: 28, 34, and 40 GHz. This will be the number of rings used in the following optimized lenses. The figure also shows the reflection coefficient obtained with CST and 2D-FEM for comparison purposes. It can be observed that this parameter also converges with the same number of rings.

V. Optimization Method

Once the number of rings is fixed, lens optimization will be explored first by allowing variations in a variable that is not typically studied, corresponding to the width of each ring w_n, while maintaining the same focal length F and lens thickness t. The optimization method employed in this work is a genetic algorithm since it allows global optimization without making large assumptions about the type of solution. The chosen implementation [30], [31] is computationally efficient and suitable for multi-objective optimization problems.

Given the high computational speed of the method, a multifrequency optimization was conducted at 33, 34, and 35 GHz to maximize the antenna gain. Following the optimization process, the lens with the highest realized gain at the design frequencies exhibited the far-field radiation pattern shown in Fig. 5a. This resulted in a maximum realized gain of 25.2 dB, a SLL of -20.9 dB, and a magnitude of the reflection coefficient equal to -10.5 dB, at 34 GHz.

The physical parameters of the lens are shown in Table I, labeled as "Case 1". The red curve in Fig. 6 shows the maximum gain for frequencies between 28 and 40 GHz. An improvement in gain between 0.5 and 1 dB has been achieved for the three optimized frequencies. However, this does not imply that the behavior is the same for the entire K_a-band, as can be seen by comparing it with the blue curve corresponding to "Case 0". This approach can be applied to enhance the gain within a specific frequency range if desired.

The design process of the GRIN lens antenna shown in Section III is based on the assumption that the feed antenna produces an ideal spherical wave, without considering the effects of a real feed antenna. The discrepancy between the ideal feed and the actual feed antenna can result in low aperture efficiency. Therefore, as a comparison, a new lens was designed using a cylindrical waveguide with corrugations as feed. When this waveguide is used as the lens feed, the maximum aperture efficiency achieved is 81%, occurring when the angle subtended by the lens and the feed is 70 degrees, i.e., for a different focal distance.

For comparison purposes, a lens with the same diameter ($10\lambda_0$) and 8 rings of constant width was designed, with the new focal length F of 62.96 mm corresponding to the subtended angle of 70 degrees. This lens is referred to as "Case 2." The lens parameters are presented in Table I, including the lens thickness t, which is now 17.1 mm, as well as the permittivities of each ring ε_n. Fig.5b shows the far-field radiation pattern in both planes at 34 GHz, and the yellow curve in Fig.6 shows the maximum gain for frequencies between 28 and 40 GHz. As can be seen, the maximum realized gain achieved is between 1 and 5.3 dB greater than that of the original lens ("Case 0").

Starting with the comparison lens ("Case 2"), we proceeded to further optimization by varying the focal length F and the lens thickness t. The primary objectives are to reduce the focal length to achieve a more compact feed-lens antenna system

Authorized licensed use limited to: Biblioteca de la Universidad de Extremadura. Downloaded on December 20,2024 at 11:14:42 UTC from IEEE Xplore. Restrictions apply.
© 2024 IEEE. Personal use is permitted, but republication/redistribution requires IEEE permission. See https://www.ieee.org/publications/rights/index.html for more information.

This article has been accepted for publication in IEEE Antennas and Wireless Propagation Letters. This is the author's version which has not been fully edited and content may change prior to final publication. Citation information: DOI 10.1109/LAWP.2024.3489426

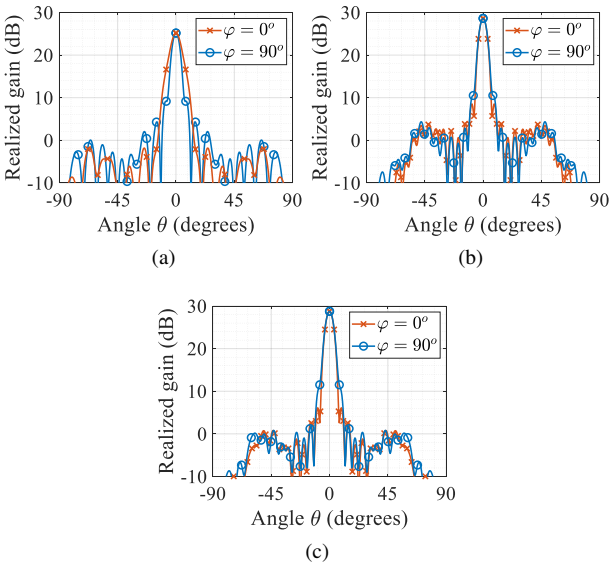

Fig. 5. Simulated E- and H-plane far-field radiation pattern at 34 GHz of the designed lens antennas: "Case 1", "Case 2" and "Case 3".

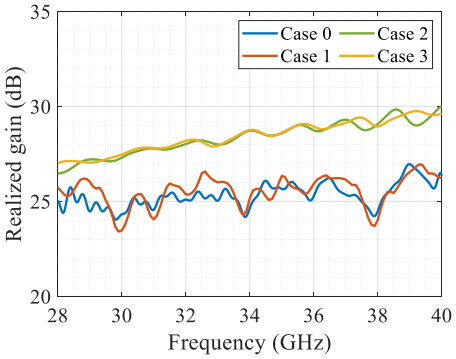

Fig. 6. Maximum realized gain for frequencies between 28 GHz and 40 GHz for the three analyzed cases, including original lens "Case 0".

and also to decrease the lens thickness. Both goals aim to be accomplished while maintaining the same level of gain.

The optimization results yielded a lens with the parameters shown in Table I, labeled "Case 3". Fig. 5c shows the far-field radiation pattern in both planes at 34 GHz, and the light-green curve in Fig. 6 shows the realized gain for frequencies between 28 and 40 GHz. As can be seen, the gain is practically the same as the one obtained in "Case 2", but with a focal length that is 13.33 mm shorter and a lens thickness that is 1.65 mm less, resulting in a more compact antenna as desired. Additionally, an aperture efficiency of 76% was achieved, as shown in Table I. The full optimization process, including frequency sweeps, was completed in approximately 10 days using a 10-year-old dual Intel Xeon E5-2670 CPU system. In contrast, performing the same optimization in CST Studio Suite would have taken around 3 years, highlighting the efficiency of the 2D FEM approach used in this work.

VI. Conclusion

This paper demonstrates the efficacy of the 2D FEM method as a powerful and time-efficient tool for analyzing electrically large structures with rotational symmetry, such as concentric ring lens antennas. The method proves invaluable for advancing the design of these structures, facilitating both simulation and optimization processes.

The ability to reduce the number of rings from 10 to 8 without compromising performance showcases how the method simplifies lens design, facilitating both analysis and manufacturing. Furthermore, integrating 2D FEM with a genetic algorithm enabled significant improvements in lens gain by optimizing ring widths, a rarely explored variable.

Additionally, the successful design of a lens antenna with reduced focal length and thickness while maintaining performance highlights the potential of the method for achieving compact designs that use less material. In Table II, a comparative analysis with other works available in the literature demonstrates the higher aperture efficiency achieved compared to other designs. It is also clear that parameters such as thickness and focal length are rarely optimized in these types of lenses, further underscoring the novelty of this approach. The capacity to simulate and optimize large lenses in a short time frame, including the simulation of thousands of configurations, underscores the impact of the method on practical applications.

In conclusion, the 2D FEM method is a robust, fast and memory-efficient tool that not only advances the study and optimization of lens antennas but also holds promise for broader applications in electrically large structures and complex optimization challenges.

TABLE I
PARAMETERS FOR EACH CASE PRESENTED, INCLUDING THE WIDTH w_n AND PERMITTIVITY OF EACH RING ε_n, AS WELL AS THE FOCAL DISTANCE F, THICKNESS OF THE LENSES t, AND APERTURE EFFICIENCY e_{ap}. THE DIMENSIONS OF w_n, F AND t ARE IN MILLIMETERS.

	w_1	w_2	w_3	w_4	w_5	w_6	w_7	w_8	w_9	w_{10}
Case 0	4.41	4.41	4.41	4.41	4.41	4.41	4.41	4.41	4.41	4.41
Case 1	4.56	9.16	4.23	4.96	2.50	4.74	5.31	8.63	-	-
Case 2	5.51	5.51	5.51	5.51	5.51	5.51	5.51	5.51	-	-
Case 3	5.51	5.51	5.51	5.51	5.51	5.51	5.51	5.51	-	-
	ε_1	ε_2	ε_3	ε_4	ε_5	ε_6	ε_7	ε_8	ε_9	ε_{10}
Case 0	12.0	11.5	10.8	9.7	8.5	7.2	5.8	4.5	3.3	2.2
Case 1	12.0	11.14	9.62	8.32	7.18	6.06	4.56	2.71	-	-
Case 2	4.0	3.93	3.80	3.63	3.28	2.80	2.31	1.72	-	-
Case 3	4.94	4.83	4.64	4.35	3.81	3.14	2.42	1.67	-	-

	Focal distance F	Thickness t	Aperture eff. e_{ap}
Case 0	29.41	11.03	29.5%
Case 1	29.41	11.03	33.3%
Case 2	62.96	17.11	75.5%
Case 3	49.69	15.46	76.1%

TABLE II
COMPARATIVE TABLE OF FLAT GRIN LENS DESIGNS FROM EXISTING LITERATURE ALONGSIDE THE RESULTS OF THE PRESENT WORK.

					Optimized	
	f_0 (GHz)	D (mm)	Gain (dB)	e_{ap}	Focal distance	Thickness
R1	28	75	25.3	70.1%	no	no
R2	15	120	21.4	38.9%	no	no
R3	30	63.5	15.2	8.3%	no	no
R4	15	120	20.5	31.6%	no	no
R5	3.5	350	20	60.8%	yes	no
R6	26	77	24	57.2%	no	no
R7	28	64.3	16	11.2%	no	no
R8	85	20	20.5	35.4%	no	no
Case 3	**34**	**88.23**	**28.8**	**76.1%**	**yes**	**yes**

Authorized licensed use limited to: Biblioteca de la Universidad de Extremadura. Downloaded on December 20,2024 at 11:14:42 UTC from IEEE Xplore. Restrictions apply.
© 2024 IEEE. Personal use is permitted, but republication/redistribution requires IEEE permission. See https://www.ieee.org/publications/rights/index.html for more information.

This article has been accepted for publication in IEEE Antennas and Wireless Propagation Letters. This is the author's version which has not been fully edited and content may change prior to final publication. Citation information: DOI 10.1109/LAWP.2024.3489426

REFERENCES

[1] O. Quevedo-Teruel, M. Ebrahimpouri, and F. Ghasemifard, "Lens antennas for 5G communications systems," *IEEE Commun. Mag.*, vol. 56, no. 7, pp. 36–41, 2018.

[2] Q. Liao, N. J. G. Fonseca, M. Camacho, A. Palomares-Caballero, F. Mesa, and O. Quevedo-Teruel, "Ray-tracing model for generalized geodesic-lens multiple-beam antennas," *IEEE Trans. Antennas Propag.*, vol. 71, no. 3, pp. 2640–2651, 2023.

[3] N. J. G. Fonseca, Q. Liao, and O. Quevedo-Teruel, "Equivalent planar lens ray-tracing model to design modulated geodesic lenses using non-Euclidean transformation optics," *IEEE Trans. Antennas Propag.*, vol. 68, no. 5, pp. 3410–3422, 2020.

[4] O. Quevedo-Teruel, Q. Liao, Q. Chen, P. Castillo-Tapia, F. Mesa, K. Zhao, and N. J. G. Fonseca, "Geodesic lens antennas for 5G and beyond," *IEEE Commun. Mag.*, vol. 60, no. 1, pp. 40–45, 2022.

[5] J.-M. Poyanco, O. Zetterstrom, P. Castillo-Tapia, N. J. G. Fonseca, F. Pizarro, and O. Quevedo-Teruel, "Two-dimensional glide-symmetric dielectric structures for planar graded-index lens antennas," *IEEE Antennas Wirel. Propag. Lett.*, vol. 20, no. 11, pp. 2171–2175, 2021.

[6] F. Doucet, N. J. G. Fonseca, E. Girard, X. Morvan, L. Le Coq, H. Legay, and R. Sauleau, "Shaped continuous parallel plate delay lens with enhanced scanning performance," *IEEE Trans. Antennas Propag.*, vol. 67, no. 11, pp. 6695–6704, 2019.

[7] N. Bartolomei, D. Blanco, F. Doucet, E. Girard, H. Legay, N. J. G. Fonseca, R. Sauleau, and M. Ettorre, "A circularly polarized parallel plate waveguide lens-like multiple-beam linear array antenna for SATCOM applications," *IEEE Access*, vol. 11, pp. 4602–4614, 2023.

[8] J. M. Poyanco, F. Pizarro, and E. Rajo-Iglesias, "3D-printed half-Maxwell fish-eye dielectric lens antenna with integrated DRA feed," in *Proc. IEEE Eur. Conf. Antennas Propag. (EuCAP)*, 2022, pp. 1–5.

[9] M. Liang, W.-R. Ng, K. Chang, K. Gbele, M. E. Gehm, and H. Xin, "A 3-D Luneburg lens antenna fabricated by polymer jetting rapid prototyping," *IEEE Trans. Antennas Propag.*, vol. 62, no. 4, pp. 1799–1807, 2014.

[10] D. Filipovic, S. Gearhart, and G. Rebeiz, "Double-slot antennas on extended hemispherical and elliptical silicon dielectric lenses," *IEEE Trans. Microw. Theory Techn.*, vol. 41, no. 10, pp. 1738–1749, 1993.

[11] C. Pfeiffer and A. Grbic, "Planar lens antennas of subwavelength thickness: Collimating leaky-waves with metasurfaces," *IEEE Trans. Antennas Propag.*, vol. 63, no. 7, pp. 3248–3253, 2015.

[12] O. Quevedo-Teruel, W. Tang, R. Mitchell-Thoma, A. Dyke, H. Dyke, L. Zhang, S. Haq, and Y. Hao, "Transformation optics for antennas: why limit the bandwidth with metamaterials?" *Sci. Rep.*, vol. 3, 2013.

[13] M. K. Saleem, H. Vettikaladi, M. A. S. Alkanhal, and M. Himdi, "Lens antenna for wide angle beam scanning at 79 GHz for automotive short range radar applications," *IEEE Trans. Antennas Propag.*, vol. 65, no. 4, pp. 2041–2046, 2017.

[14] R. K. Arya, S. Zhang, Y. Vardaxoglou, W. Whittow, and R. Mittra, "3D-printed millimeter wave lens antenna," in *2017 10th Global Symposium on Millimeter-Waves*, 2017, pp. 172–174.

[15] T. Whittaker, S. Zhang, A. Powell, C. J. Stevens, J. Y. C. Vardaxoglou, and W. Whittow, "3D printing materials and techniques for antennas and metamaterials: A survey of the latest advances," *IEEE Antennas Propag. Mag.*, vol. 65, no. 3, pp. 10–20, 2023.

[16] J.-M. Poyanco, F. Pizarro, and E. Rajo-Iglesias, "3D-printing for transformation optics in electromagnetic high-frequency lens applications," *Materials*, vol. 13, no. 12, 2020.

[17] S. Zhang, R. K. Arya, S. Pandey, Y. Vardaxoglou, W. Whittow, and R. Mittra, "3D-printed planar graded index lenses," *IET Microwaves, Antennas & Propagation*, vol. 10, no. 13, pp. 1411–1419, 2016.

[18] T. McManus, R. Mittra, and C. Pelletti, "A comparative study of flat and profiled lenses," in *Proc. IEEE Int. Symp. Antennas Propag. (ISAP)*, 2012, pp. 1–2.

[19] S. Zhang, Y. Vardaxoglou, W. Whittow, and R. Mittra, "3D-printed graded index lens for RF applications," in *2016 International Symposium on Antennas and Propagation (ISAP)*, 2016, pp. 90–91.

[20] A. Piroutiniya, M. H. Rasekhmanesh, J. L. Masa-Campos, J. López-Hernández, E. García-Marín, A. Tamayo-Domínguez, P. Sánchez-Olivares, and J. A. Ruiz-Cruz, "Beam steering 3D printed dielectric lens antennas for millimeter-wave and 5G applications," *Sensors*, vol. 23, no. 15, 2023.

[21] M. Kunkle, R. Allen, and K. Durbhakula, "Ultrawideband gain enhancement using 3D printed dielectric gradient refractive index lens," in *2023 IEEE International Symposium on Antennas and Propagation and USNC-URSI Radio Science Meeting (USNC-URSI)*, 2023, pp. 1689–1690.

[22] E. Garcia-Marin, D. S. Filipovic, J. L. Masa-Campos, and P. Sanchez-Olivares, "Ka-band multi-beam planar lens antenna for 5G applications," in *2020 14th European Conference on Antennas and Propagation (EuCAP)*, 2020, pp. 1–5.

[23] Y. Kim, D. A. Pham, R. Phon, and S. Lim, "Lightweight 3D-printed fractal gradient-index lens antenna with stable gain performance," *Fractal and Fractional*, vol. 6, no. 10, p. 551, 2022.

[24] J. Melendro-Jimenez, P. Sanchez-Olivares, A. Tamayo-Dominguez, X. Sun, and J. M. Fernandez-Gonzalez, "3D printed directive beam-steering antenna based on gradient index flat lens with an integrated polarizer for dual circular polarization at W-band," *IEEE Transactions on Antennas and Propagation*, vol. 71, no. 1, pp. 1059–1064, 2023.

[25] J.-M. Poyanco, F. Pizarro, and E. Rajo-Iglesias, "Cost-effective wide-band dielectric planar lens antenna for millimeter wave applications," *Sci. Rep.*, vol. 12, no. 1, 2022.

[26] J. M. Gil, J. Monge, J. Rubio, and J. Zapata, "A CAD-oriented method to analyze and design radiating structures based on bodies of revolution by using finite elements and generalized scattering matrix," *IEEE Trans. Antennas Propag.*, vol. 54, no. 3, pp. 899–907, 2006.

[27] J. Rubio, M. Gonzalez, and J. Zapata, "Analysis of cavity-backed microstrip antennas by a 3-D finite element/segmentation method and a matrix Lanczos-Pade algorithm (SFELP)," *IEEE Antennas Wirel. Propag. Lett.*, vol. 1, pp. 193–195, 2002.

[28] J. Webb, "Hierarchal vector basis functions of arbitrary order for triangular and tetrahedral finite elements," *IEEE Trans. Antennas Propag.*, vol. 47, no. 8, pp. 1244–1253, 1999.

[29] J. E. Hansen, Ed., *Spherical Near-field Antenna Measurements*, ser. Electromagnetic Waves. Institution of Engineering and Technology, 1988.

[30] K. Deb, A. Pratap, S. Agarwal, and T. Meyarivan, "A fast and elitist multiobjective genetic algorithm: NSGA-II," *IEEE Trans. Evol. Comput.*, vol. 6, no. 2, pp. 182–197, 2002.

[31] "NSGA - II: A multi-objective optimization algorithm." [Online]. Available: https://www.mathworks.com/matlabcentral/fileexchange/10429-nsga-ii-a-multi-objective-optimization-algorithm.

Authorized licensed use limited to: Biblioteca de la Universidad de Extremadura. Downloaded on December 20,2024 at 11:14:42 UTC from IEEE Xplore. Restrictions apply.
© 2024 IEEE. Personal use is permitted, but republication/redistribution requires IEEE permission. See https://www.ieee.org/publications/rights/index.html for more information.